

Subtype-Aware Registration of Longitudinal Electronic Health Records

Xin Gai^{1*}, Shiyi Jiang^{1†}, and Anru R. Zhang^{2‡}

Abstract

Electronic Health Records (EHRs) contain extensive patient information that can inform downstream clinical decisions, such as mortality prediction, disease phenotyping, and disease onset prediction. A key challenge in EHR data analysis is the temporal gap between when a condition is first recorded and its actual onset time. Such timeline misalignment can lead to artificially distinct biomarker trends among patients with similar disease progression, undermining the reliability of downstream analysis and complicating tasks like disease subtyping. To address this challenge, we provide a subtype-aware timeline registration method that leverages data projection and discrete optimization to simultaneously correct timeline misalignment and improve disease subtyping. Through simulation and real-world data analyses, we demonstrate that the proposed method effectively aligns distorted observed records with the true disease progression patterns, enhancing subtyping clarity and improving performance in downstream clinical analyses.

*Department of Biostatistics, Vanderbilt University

†Department of Electrical & Computer Engineering, Duke University

‡Department of Biostatistics & Bioinformatics and Department of Computer Science, Duke University

¹Equal contribution. ²Corresponding author. E-mail: anru.zhang@duke.edu

1 Introduction

Electronic Health Records (EHR) are digitized collections of patient hospital information, encompassing data such as demographic, lab measurements, diagnoses, and medications. Data collected from intensive care unit (ICU) patients are of particular interest in clinical research due to their high frequency and timely collection. These data contain crucial information for executing timely disease interventions, managing patient care, and facilitating various downstream clinical decisions [1, 2, 3].

However, a significant challenge in utilizing EHR data lies in the temporal gap between when a condition is first recorded and its actual onset time. For example, a patient with pneumonia might be admitted to the hospital at the congestion stage (stage one) [4], while another patient might delay hospital visitation until a later stage due to factors like insurance coverage or personal health beliefs [5], resulting in unobserved data for the initial stages of disease progression. Conventional analyses on EHR data often overlook this misalignment of timelines, potentially leading to biased modeling results. Therefore, it is crucial to address this issue by developing methods that can effectively align observed EHR timelines with the true underlying disease progression.

1.1 Registration in the Literature

This need for timeline alignment is closely related to the problem of curve registration in functional data analysis, which seeks to align curves so that key features are properly synchronized across subjects [6, 7, 8]. In engineering, this problem is often referred to as time warping [9, 10]. Early methods aligned curves to a single baseline, using approaches like self-modeling nonlinear regression [11, 12] or template selection through functional principal component analysis (FPCA) [13], e.g., [14]. Subsequent work has explored a variety of alignment strategies. For instance, [15] proposed equating curve “moments” to capture local and global features, while [16] introduced a similarity index to iteratively register functional

data. Other studies have applied Fisher-Rao metric-based approaches [17, 18, 19], computationally efficient techniques tailored for exponential family functional data [20, 21, 22], and pairwise warping strategies [23]. These approaches have been applied to a range of applications, including house price modeling [24], accelerometric activity data [25], and speech analysis [26]. However, since EHR data are often highly heterogeneous, sparse, noisy, and irregular, traditional curve registration methods are often not directly applicable.

Furthermore, some studies have explored combining curve registration with clustering to account for the latent subgroups among subjects. [27] used an EM algorithm with B-splines, while [28] employed a Bayesian framework that accommodates flexible warping functions. Yet, these methods often rely on specific data distributions that may not align with the complexities of EHR datasets.

To the best of our knowledge, [29] made a first attempt to address EHR-specific registration. They proposed aligning EHR trajectories by estimating time shifts to a common disease progression template. They assumed that all patients with a disease of interest share a common disease progression template and proposed a registration method using alternating optimization to align observed EHR data to this shared template. Despite its novelty, this approach has several limitations: (1) the reliance on linear interpolation and extrapolation for imputing missing data can lead to inaccurate estimations, particularly in sparsely observed EHR datasets; (2) the high computational burden of timeline registration for imputed curves becomes impractical for large patient cohorts; and (3) the assumption of a single progression template fails to account for the significant heterogeneity in diseases, where patients may follow distinct progression patterns.

In summary, while various registration and clustering methods exist, they remain constrained by assumptions unsuitable for EHR data’s sporadic and heterogeneous nature. These challenges necessitate the development of a new timeline registration method that effectively address the distinct complexities of EHR datasets, including data sparsity, diverse disease subtypes, and large patient populations.

1.2 Our Contributions

To address the limitations mentioned above, this paper introduces an efficient and effective subtype-aware registration method tailored for electronic health records data. Our approach recognizes that patients can be grouped into subtypes, each potentially following a different disease progression pattern. Specifically, we consider an EHR dataset comprising N subjects, where each subject i has longitudinal data $\{(t_{ik}, X_i(t_{ik})) \mid k = 1, 2, \dots, T_i\}$. Here, t_{ik} denotes the observation times within the domain of interest $[T_{\min}, T_{\max}]$, $X_i(t_{ik})$ represents the corresponding observations, and T_i is the number of observations for subject i . The observation times and the number of observations vary significantly across subjects. See the left panel of Figure 1 for an illustrative example on trajectories. The subjects belong to multiple disjoint subtypes $\mathcal{P}_1, \dots, \mathcal{P}_K$, where each subtype \mathcal{P}_k contains patients with similar disease progression patterns.

Our goal is to align the timelines of subjects within each subtype more closely to each other by estimating individual time shifts τ_i and clustering labels π_i such that the shifted data $X_i(t - \tau_i)$ align optimally for all i in subtype \mathcal{P}_k . Recognizing that outliers commonly occur in the electronic health records [30], we also aim to ensure robustness against them in our procedure.

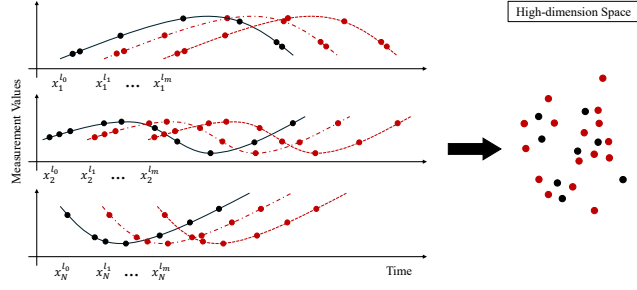
To achieve this, we transform the observed longitudinal data and all possible time shifts using cubic B-spline regression, reducing the data’s dimensionality and enabling accelerated computation. We then cluster the data in the transformed space and iteratively update the clusters by selecting the time shifts that minimize the distance to cluster centroids. Each cluster in the transformed space is considered a potential subtype of the disease of interest. By focusing on minimizing intra-cluster variance, our method effectively and robustly captures the heterogeneity of disease progression patterns while maintaining robustness to outliers. In summary, our proposed method overcomes the limitations of existing approaches by incorporating subtype awareness, improving computational efficiency, and enhancing ro-

bustness to data sparsity and outliers. We present a simulation example in Figure 1 to demonstrate the effectiveness of timeline registration. The left panel shows the observed data and the right panel shows the unobserved underlying patterns, which include two unknown subtypes of trajectories marked in blue and red. The recovered trajectories after applying the proposed timeline registration are displayed in the center panel of Figure 1. Further discussions on the simulation studies are deferred to Section 3.

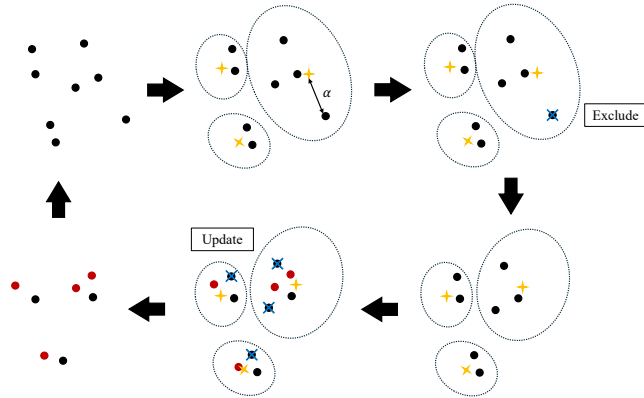


Figure 1: Simulation 1 Trajectories: Left: Observed trajectories with unregistered timelines and unknown subtypes. Right: True trajectories with subtypes indicated by colors. Middle: Trajectories after applying the proposed timeline registration, with recovered subtypes marked by colors.

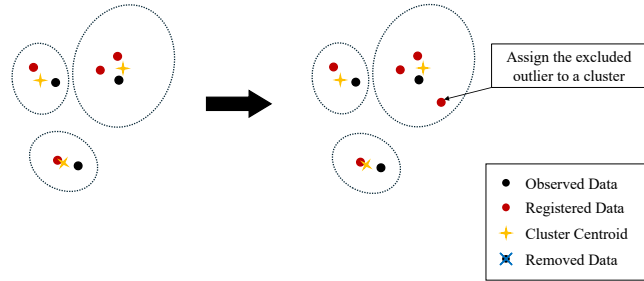
We evaluate our algorithm through extensive numerical studies. In six simulated datasets, our algorithm successfully realigned the observed data to the ground truth with less than one day of error in over 90% subjects. This realignment resulted in an enhanced separation between patient clusters, as measured by the Silhouette coefficient, from both data-driven and clinical perspectives. Furthermore, the realigned EHR data improved the predictive accuracy for severe AKI patients by 3–5%, demonstrating the effectiveness of the registered data in supporting accurate prediction modeling.



(a) Step 1: Time Series Transformation Using Cubic B-spline Regression



(b) Step 2: Iterations



(c) Step 3: Finalization

Figure 2: This figure illustrates subtype-aware registration using longitudinal EHR data. Black lines and dots represent the current curves, observations, and their low-dimensional embeddings. Red lines and dots indicate curves and observations that include potential time shifts under consideration. Blue dots represent potential outliers that were excluded from centroid evaluation for the time being.

2 Method for Subtype-Aware Registration of EHR

Through this paper, we denote $[N] = \{1, \dots, N\}$ for any integer $N \geq 1$. Let $|\mathcal{C}|$ be the cardinality of any set \mathcal{C} . The Euclidean norm or the ℓ_2 norm of a vector x is denoted as $\|\cdot\|$, i.e., $\|x\| = \sqrt{\sum_i x_i^2}$. Then, $\|\mathbf{u} - \mathbf{v}\|$ represents the Euclidean distance between two vectors \mathbf{u} and \mathbf{v} .

Next, we propose the EHR registration algorithm shown in Figure 2, which consists of three main steps, detailed in the following subsections. The pseudo-code for each step is provided in Algorithms 1, 2, and 3.

Step 1: Time Series Transformation Using Cubic B-spline Regression

In this step, we apply cubic B-spline regression [31, 32] to perform time series transformation. This technique models longitudinal data with flexible and smooth approximations, yielding a low-dimensional representation.

Specifically, we introduce q internal knots, denoted as $\{\tau_1, \dots, \tau_q\}$, within the overall time domain $[T_{\min}, T_{\max}]$. Based on these knots, we construct $p = q + 3$ basis functions for cubic splines $B_{j,3}(t)$ recursively as follows.

First, the zeroth-degree basis functions $B_{j,0}(t)$ are defined as piecewise constants:

$$B_{j,0}(t) = \begin{cases} 1 & \text{if } t \in [\tau_j, \tau_{j+1}), \\ 0 & \text{otherwise.} \end{cases}$$

Then, for $m = 1, 2, 3$, the higher-degree basis functions are constructed recursively:

$$B_{j,m}(t) = \frac{t - \tau_j}{\tau_{j+m} - \tau_j} B_{j,m-1}(t) + \frac{\tau_{j+m+1} - t}{\tau_{j+m+1} - \tau_{j+1}} B_{j+1,m-1}(t).$$

For more details about B-splines, readers are referred to [33].

We perform B-spline regression using ridge regression (which provides more robustness) to fit both the original and time-shifted observations for each subject $i = 1, \dots, N$. Specifically,

we pre-specify a set of potential shift positions $\Lambda = \{l_0, l_1, \dots, l_m\}$, where $l_0 = 0$ means no shift. For each $i = 1, \dots, N$ and $l \in \Lambda$, we perform ridge regression $X_i(t - l) \sim B_{j,3}(t)$ by evaluating the following estimator:

$$\widehat{\beta}_{i,l} = \arg \min_{\beta_{i,l}} \left\{ \sum_{\substack{k=1 \\ T_{\min} \leq t_{ik} - l \leq T_{\max}}}^{T_i} \left(X_i(t_{ik} - l) - \sum_{j=1}^p \beta_{ij} B_{j,3}(t_{ik}) \right)^2 + \lambda \sum_{j=1}^p \beta_{ij}^2 \right\},$$

where λ is the tuning parameter that controls the penalization level, and $\widehat{\beta}_{i,l} = (\widehat{\beta}_{i1}, \widehat{\beta}_{i2}, \dots, \widehat{\beta}_{ip})$ is the vector of estimated coefficients. In this way, the underlying structure and dynamics of the longitudinal data are reduced to p coefficients. This cubic B-spline regression yields the following low-dimensional embedding:

$$\{(t_{ik}, X_i(t_{ik})) \mid k = 1, 2, \dots, T_i\} \longrightarrow \widehat{\beta}_{i,l}.$$

We compute and store these low-dimensional representations for all subjects and potential shifts into a tensor $\Omega \in \mathbb{R}^{N \times |\Lambda| \times p}$:

$$\Omega_{[i,l,:]} = \widehat{\beta}_{i,l}, \quad \text{for } i = 1, \dots, N; \quad l \in \Lambda.$$

Step 2: Iterations

We set the initial time shifts as $\delta_i^{(0)} = 0$ for all $i = 1, \dots, N$. Next, we run the following steps for $t = 1, 2, \dots$:

1. **Clustering with Optimal Number of Clusters.** For each candidate number of clusters $k \in \{2, \dots, M\}$, we conduct clustering (e.g., k -means, k -medoids) with k clusters on the low-dimensional representations with time shifts $\delta_i^{(t-1)}$: $\{\Omega_{i,\delta_i^{(t-1)}}\}_{i=1}^N$. When $t = 1$, the data is the original longitudinal dataset without time shifts.

We determine the number of clusters $K^{(t)}$ by selecting the k that maximizes the average Silhouette coefficient [34]:

$$K^{(t)} = \arg \max_{k \in \{2, \dots, M\}} s(k), \quad s(k) = \frac{1}{N} \sum_{i=1}^N s(i, k), \quad (1)$$

where $s(i, k)$ is the Silhouette coefficient for subject i when the number of clusters is k .

This results in $K^{(t)}$ clusters of the subjects: $\{\mathcal{C}_1^{(t)}, \dots, \mathcal{C}_{K^{(t)}}^{(t)}\} \subseteq [N]$, where $\mathcal{C}_i^{(t)} \cap \mathcal{C}_j^{(t)} = \emptyset$ for all $i \neq j$.

2. Iterative Updates. For each cluster $k = 1, \dots, K^{(t)}$, we perform:

- Compute the centroid of cluster $\mathcal{C}_k^{(t)}$:

$$\bar{\beta}_k^{(t)} = \frac{1}{|\mathcal{C}_k^{(t)}|} \sum_{i \in \mathcal{C}_k^{(t)}} \Omega_{i, \delta_i^{(t-1)}}.$$

- Calculate the Euclidean distance between each point in the cluster and the centroid:

$$d_i = \left\| \Omega_{i, \delta_i^{(t-1)}} - \bar{\beta}_k^{(t)} \right\|, \quad \forall i \in \mathcal{C}_k^{(t)}.$$

- Select the subset $\mathcal{S}_k^{(t)}$ of points corresponding to the smallest $\left\lceil \alpha |\mathcal{C}_k^{(t)}| \right\rceil$ distances:

$$\mathcal{S}_k^{(t)} = \left\{ i \in \mathcal{C}_k^{(t)} \mid d_i \text{ is among the smallest } \left\lceil \alpha |\mathcal{C}_k^{(t)}| \right\rceil \text{ values} \right\},$$

where $0 < \alpha \leq 1$ is a predefined proportion.

- Recompute the centroid using only the selected points:

$$\bar{\gamma}_k^{(t)} = \frac{1}{|\mathcal{S}_k^{(t)}|} \sum_{i \in \mathcal{S}_k^{(t)}} \Omega_{i, \delta_i^{(t-1)}}.$$

This step removes potential outliers ($\mathcal{C}_k^{(t)} \setminus \mathcal{S}_k^{(t)}$) from the centroid computation, enhancing robustness.

- Update the time shifts for each subject $i \in \mathcal{C}_k^{(t)}$ by finding the shift $\delta_i^{(t)} \in \Lambda$ that minimizes the distance to the updated centroid:

$$\delta_i^{(t)} = \arg \min_{\delta \in \Lambda} \left\| \Omega_{i, \delta} - \bar{\gamma}_k^{(t)} \right\|^2.$$

3. Stopping Criterion. We employ stopping criteria to ensure efficient convergence and prevent excessive computation. Based on the initial clustering $\{\mathcal{C}_1^{(1)}, \dots, \mathcal{C}_{K^{(1)}}^{(1)}\}$, we evaluate the average Silhouette coefficient $s(K^{(1)})$ using Equation (1). The maximum number of iterations I is set as:

$$I = \begin{cases} I_{\text{small}} & \text{if } s(K^{(1)}) > \tau, \\ I_{\text{large}} & \text{if } s(K^{(1)}) \leq \tau, \end{cases}$$

where τ is a predefined threshold.

We terminate the iterations when:

$$\{K^{(t)} = K^{(t-1)} \text{ and } t > I\} \quad \text{or} \quad \{t > 2I\}.$$

The condition $t > 2I$ provides a safeguard to ensure termination even if convergence is not achieved within the expected number of iterations.

2.1 Step 3: Finalization

Upon termination at iteration $t = t_{\text{final}}$, we address the data points not selected during the last iteration. For each cluster k , consider the set of unselected points: $\mathcal{C}_k^{(t_{\text{final}})} \setminus \mathcal{S}_k^{(t_{\text{final}})}$, where $\mathcal{S}_k^{(t_{\text{final}})}$ denotes the subset of selected points within cluster k after the final iteration.

For each unselected point $j \in \mathcal{C}_k^{(t_{\text{final}})} \setminus \mathcal{S}_k^{(t_{\text{final}})}$, find the optimal shift δ_j^* and assign it to the most appropriate cluster center by solving:

$$\delta_j^*, k'^* = \arg \min_{\delta_j \in \Lambda, k'=1, \dots, K^{(t_{\text{final}})}} \left\| \Omega_{j, \delta_j} - \bar{\gamma}_{k'}^{(t_{\text{final}})} \right\|.$$

This assigns j to $\mathcal{S}_{k'}^{(t_{\text{final}})}$ and shift state that best represents it.

The final output of the algorithm is the number of clusters $\widehat{K}^{t_{\text{final}}}$, the set of shift states, and clusters for all subjects:

$$\{\delta_i^* : i = 1, 2, \dots, N\} \quad \text{and} \quad \{\mathcal{S}_k^{(t_{\text{final}})}\}_{k \in \widehat{K}^{(t_{\text{final}})}}.$$

The overall pseudo code is summarized in Algorithms 1-3.

Algorithm 1 Time Series Clustering with Dynamic Time Shifts: Step 1: Transformation

Require: Longitudinal data $\{(t_{ik}, X_i(t_{ik})) \mid i = 1, \dots, N; k = 1, \dots, T_i\}$, Potential shift positions $\Lambda = \{l_0, l_1, \dots, l_m\}$, Maximum number of clusters M , predefined threshold τ , Parameters α , I_{small} , I_{large} , penalization parameter λ .

Ensure: Optimal shift states $\{\delta_i^* \mid i = 1, 2, \dots, N\}$ and clusters $\{\mathcal{C}_k^{(t_{\text{final}})}\}$

- 1: Introduce internal knots $\{\tau_1, \dots, \tau_q\}$ in $[T_{\min}, T_{\max}]$
- 2: Construct cubic B-spline basis functions $B_{j,3}(t)$
- 3: **for** each subject $i = 1$ to N **do**
- 4: **for** each shift $l \in \Lambda$ **do**
- 5: Perform ridge regression to obtain coefficients:

$$\widehat{\beta}_{i,l} = \arg \min_{\beta_{i,l}} \left\{ \sum_{\substack{k=1 \\ T_{\min} \leq t_{ik} - l \leq T_{\max}}}^{T_i} \left(X_i(t_{ik} - l) - \sum_{j=1}^p \beta_{ij} B_{j,3}(t_{ik}) \right)^2 + \lambda \sum_{j=1}^p \beta_{ij}^2 \right\}$$

- 6: Store coefficients in tensor $\Omega_{[i,l,:]} = \widehat{\beta}_{i,l}$
 - 7: **end for**
 - 8: **end for**
-

Algorithm 2 Step 2: Iterative Clustering and Time Shift Adjustment

- 1: Initialize time shifts $\delta_i^{(0)} = 0$ for all i . Set iteration counter $t \leftarrow 1$
 - 2: **repeat**
 - 3: **for** each k in $\{2, \dots, M\}$ **do**
 - 4: Perform clustering with k clusters on $\{\Omega_{i, \delta_i^{(t-1)}}\}_{i=1}^N$
 - 5: Compute average Silhouette coefficient $s(k)$ using (1)
 - 6: **end for**
 - 7: Select optimal number of clusters: $K^{(t)} = \arg \max_k s(k)$; obtain clusters $\{\mathcal{C}_1^{(t)}, \dots, \mathcal{C}_{K^{(t)}}^{(t)}\}$
 - 8: **for** each cluster $k = 1$ to $K^{(t)}$ **do**
 - 9: Compute centroid: $\bar{\beta}_k^{(t)} = \sum_{i \in \mathcal{C}_k^{(t)}} \Omega_{i, \delta_i^{(t-1)}} / |\mathcal{C}_k^{(t)}|$
 - 10: Calculate distances $d_i = \left\| \Omega_{i, \delta_i^{(t-1)}} - \bar{\beta}_k^{(t)} \right\|$ for $i \in \mathcal{C}_k^{(t)}$
 - 11: Select subset $\mathcal{S}_k^{(t)}$ of points with smallest $\left[\alpha |\mathcal{C}_k^{(t)}| \right]$ distances
 - 12: Recompute centroid: $\bar{\gamma}_k^{(t)} = \sum_{i \in \mathcal{S}_k^{(t)}} \Omega_{i, \delta_i^{(t-1)}} / |\mathcal{S}_k^{(t)}|$
 - 13: **end for**
 - 14: **for** each subject $i = 1$ to N **do**
 - 15: Update time shift: $\delta_i^{(t)} = \arg \min_{\delta \in \Lambda} \left\| \Omega_{i, \delta} - \bar{\gamma}_k^{(t)} \right\|^2$, where k is the cluster containing subject i
 - 16: **end for**
 - 17: Update $t \leftarrow t + 1$
 - 18: **Check Stopping Criteria**
 - 19: **if** $K^{(t)} = K^{(t-1)}$ **and** $t > I$ **then**
 - 20: **Terminate Iteration**
 - 21: **else if** $t > 2I$ **then**
 - 22: **Terminate Iteration (Hard Stop)**
 - 23: **end if**
 - 24: **until** Termination condition is met
-

Algorithm 3 Step 3: Iterative Clustering and Time Shift Adjustment

- 1: **for** each cluster k **do**
- 2: **for** each unselected point $j \in \mathcal{C}_k^{(t_{\text{final}})} \setminus \mathcal{S}_k^{(t_{\text{final}})}$ **do**
- 3: Assign optimal shift and cluster by evaluating

$$\delta_j^*, k'^* = \underset{\delta_j \in \Lambda, k' = 1, \dots, K^{(t_{\text{final}})}}{\operatorname{arg\,min}} \left\| \Omega_{j, \delta_j} - \bar{\gamma}_{k'}^{(t_{\text{final}})} \right\|.$$

Then reassign j to cluster $\mathcal{S}_{k'^*}^{(t_{\text{final}})}$.

- 4: **end for**
 - 5: **end for**
 - 6: **Output** final shift amounts $\{\delta_i^* \mid i = 1, 2, \dots, N\}$ and clusters $\{\mathcal{S}_k^{(t_{\text{final}})}\}$
-

3 Simulations

In this section, we conduct simulation studies across six scenarios to evaluate the effectiveness of our proposed algorithm. These scenarios covered a variety of different longitudinal data structures, including different shapes, different means, and their combinations. The objective is to assess the proposed algorithm’s ability to correctly recover the true temporal positions of these longitudinal data under various conditions. Next, we will describe the common setup, then discuss specific designs, and finally discuss the simulation results.

Common Simulation Setup. *Data Generation:* For each subject i (where $i = 1, 2, \dots, 1000$), the observation time points t_{ij} (where $j = 1, 2, \dots, 28$) were randomly drawn from a continuous uniform distribution over the interval $[1, 21]$ ($t_{ij} \sim \text{Uniform}(1, 21)$). These time points were then sorted in ascending order for each subject. In all scenarios, the noise terms ϵ_{ij} were randomly drawn from a normal distribution $\epsilon_{ij} \sim N(0, 0.8^2)$.

Temporal Misalignment Simulation: In all scenarios, each subject was assigned a time shift to simulate the delay between the onset of illness and hospital admission. Specifically, in

each scenario, 60% of the subjects in a group had a time shift of 0, representing patients who were admitted to the hospital immediately upon illness onset or were promptly transferred from general wards to the ICU after the onset of severe symptoms. The remaining 40% of subjects were assigned a random time shift ranging from 1 to 4 days (integers), simulating a delay of 1 to 4 days between illness onset and hospital admission. After applying the time shifts, any observations with time points less than 1 were removed to simulate the missing data during the “onset-to-admission” period when patients experience a delay in hospital admission. Additionally, observations with time points greater than 17 were removed to ensure a consistent study time window across all individuals.

Algorithm Parameter Settings: We fix 2 internal knots at 8 and 13. The potential shift positions Λ were set to $\{0, 1, 2, 3, 4\}$. The range of cluster numbers was set to $\{2, 3, \dots, 8\}$, i.e., $M = 8$. The selection proportion α was set to 0.95, the threshold τ was set to 0.45, and the maximum iteration numbers were set to $I_{\text{small}} = 1$ and $I_{\text{large}} = 10$. We employ k -medoids as the clustering method employed given its robustness to outliers [35].

Scenario 1: This scenario involves two types of trajectories that are similar in shape but have significant differences in mean, defined as follows:

$$\text{Group 1 (500 subjects): } Y_i^{(1)}(t_{ij}) = 20 + 3 \sin(0.6(t_{ij} + 4)) + \epsilon_{ij};$$

$$\text{Group 2 (500 subjects): } Y_i^{(2)}(t_{ij}) = 17 + 3 \sin(0.6(t_{ij} + 4)) + \epsilon_{ij}.$$

In this setting, the trajectories from Group 1 had a higher mean level compared to Group 2, while the overall shape of their trajectories, dictated by the sinusoidal base sequence, remained similar. This setup allows us to evaluate the algorithm’s ability to distinguish between groups with different mean levels but similar temporal patterns.

Scenario 2: This scenario involves two types of trajectories with distinct shape differences but similar overall means.

$$\text{Group 1 (500 subjects): } Y_i^{(1)}(t_{ij}) = 17 + 2 \sin(0.6(t_{ij} + 4)) + \epsilon_{ij};$$

$$\text{Group 2 (500 subjects): } Y_i^{(2)}(t_{ij}) = 2t_{ij} + 3 \sin(0.6(t_{ij} + 4)) + \epsilon_{ij}.$$

While both groups have similar overall means, Group 1 follows a sinusoidal pattern, whereas Group 2 exhibits a combination of a sinusoidal pattern and a linear trend.

Scenario 3: This scenario involves three types of trajectories defined as follows:

$$\text{Group 1 (300 subjects): } Y_i^{(1)}(t_{ij}) = 20 + 3 \sin(0.6(t_{ij} + 4)) + \epsilon_{ij};$$

$$\text{Group 2 (400 subjects): } Y_i^{(2)}(t_{ij}) = 17 + 3 \sin(0.6(t_{ij} + 4)) + \epsilon_{ij};$$

$$\text{Group 3 (300 subjects): } Y_i^{(3)}(t_{ij}) = 16 + 0.5t_{ij} + 3 \sin(0.9(t_{ij} + 4)) + \epsilon_{ij}.$$

In summary, Groups 1 and 2 have similar shapes but different means, while Group 3 has a different shape that overlaps with the first two groups. This scenario helps evaluate the algorithm's ability to distinguish between groups with both shape and mean differences.

Scenario 4: This scenario involves four types of trajectories with shape differences and overlaps:

$$\text{Group 1 (250 subjects): } Y_i^{(1)}(t_{ij}) = 24 + 3 \sin(0.6(t_{ij} + 4)) + \epsilon_{ij};$$

$$\text{Group 2 (250 subjects): } Y_i^{(2)}(t_{ij}) = 17 + 3 \sin(0.6(t_{ij} + 4)) + \epsilon_{ij};$$

$$\text{Group 3 (250 subjects): } Y_i^{(3)}(t_{ij}) = 38 - 0.5t_{ij} + 4 \sin(0.9(t_{ij} + 3)) + \epsilon_{ij};$$

$$\text{Group 4 (250 subjects): } Y_i^{(4)}(t_{ij}) = 21 + 0.9t_{ij} + 3 \sin(0.6(t_{ij} + 4)) + \epsilon_{ij}.$$

In this scenario, Groups 1 and 2 have similar shapes but different means, while Groups 3 and 4 exhibit different shapes that overlap with each other and the first two groups.

Scenario 5: This scenario includes 4 groups of trajectories and each group includes 250 subjects. The trajectories of each group is generated as follows:

$$\text{Group 1 (250 subjects): } Y_i^{(1)}(t_{ij}) = 24 + 3 \sin(0.6(t_{ij} + 4)) + \epsilon_{ij}^{(1)};$$

$$\text{Group 2 (250 subjects): } Y_i^{(2)}(t_{ij}) = 17 + 3 \sin(0.6(t_{ij} + 4)) + \epsilon_{ij}^{(2)};$$

$$\text{Group 3 (250 subjects): } Y_i^{(3)}(t_{ij}) = 28 - 0.5t_{ij} + 4 \sin(0.9(t + 3)) + \epsilon_{ij}^{(3)};$$

$$\text{Group 4 (250 subjects): } Y_i^{(4)}(t_{ij}) = 21 - 0.5t_{ij} + 4 \sin(0.9(t + 3)) + \epsilon_{ij}^{(4)}.$$

In this scenario, the trajectories in Groups 1 and 2 share one shape with different means, while Groups 3 and 4 share another shape with different means. This scenario helps evaluate the algorithm's ability to distinguish between overlapping groups with similar shapes but different mean levels.

Scenario 6: This scenario includes 4 groups of trajectories and each group includes 250 subjects. The trajectories of each group is generated as follows:

$$\text{Group 1 (250 subjects): } Y_i^{(1)}(t_{ij}) = 23 + 3 \sin(0.6(t_{ij} + 4)) + \epsilon_{ij};$$

$$\text{Group 1 (250 subjects): } Y_i^{(2)}(t_{ij}) = 17 + 3 \sin(0.6(t_{ij} + 4)) + \epsilon_{ij};$$

$$\text{Group 1 (250 subjects): } Y_i^{(3)}(t_{ij}) = 20 + 3 \sin(0.6(t_{ij} + 4)) + \epsilon_{ij};$$

$$\text{Group 1 (250 subjects): } Y_i^{(4)}(t_{ij}) = 25 - 0.5t_{ij} + 4 \sin(0.9(t_{ij} + 3)) + \epsilon_{ij}.$$

In summary, Groups 1, 2, and 3 share a similar shape with different means, while Group 4 has a distinctly different shape but overlaps with other types. This scenario helps evaluate the algorithm's ability to distinguish between groups with both shape and mean differences, including overlapping patterns.

We use four metrics to evaluate the performance of the algorithm: Accuracy Rate refers to the proportion of subjects for whom the algorithm successfully recovered the correct temporal positions of their longitudinal data; Probability of Error ≤ 1 Day refers to the proportion of subjects with a result error of less than or equal to 1 day; Mean Absolute Error (MAE) represents the average time difference between the recovered temporal positions and the

Scenario	Rate of Exact Recovery	Rate of Recovery Error ≤ 1	MAE (days)	Runtime (min)
1 (2 clusters)	69.0% [62.0%, 83.9%]	92.0% [84.9%, 99.5%]	0.40 [0.17, 0.55]	3.13 [1.22, 7.42]
2 (2 clusters)	75.8% [73.1%, 80.0%]	94.5% [90.6%, 98.0%]	0.35 [0.24, 0.49]	1.24 [0.86, 1.93]
3 (3 clusters)	74.0% [71.1%, 78.1%]	91.5% [90.5%, 93.1%]	0.40 [0.34, 0.43]	1.25 [0.87, 1.93]
4 (4 clusters)	69.2% [61.3%, 79.6%]	97.1% [95.7%, 98.5%]	0.37 [0.28, 0.47]	2.63 [1.86, 5.46]
5 (4 clusters)	65.2% [50.7%, 75.9%]	90.6% [87.9%, 93.2%]	0.60 [0.45, 0.77]	4.56 [1.29, 7.57]
6 (4 clusters)	76.0% [69.8%, 80.7%]	93.9% [89.8%, 96.4%]	0.41 [0.30, 0.58]	1.69 [1.14, 2.07]

Table 1: Simulation Results: We present the average value and 95% confidence interval for the rate of exact recovery, rate of recovery error, mean absolute value, and runtime

correct temporal positions for all subjects, and the Runtime indicates the time taken for the algorithm to run once on the simulated dataset. The simulation results, which present the average values and 95% confidence intervals for all four metrics over 500 runs, are shown in Table 1. The visualizations of the simulation results can be found in Figures 1, 3, 4, 5, 6, and 7 in the Appendix.

In summary, our algorithm effectively recovered the temporal positions from the simulated data across all six scenarios. The evaluation metrics show similar values regardless of the complexity of the scenario, indicating the robustness of our algorithm. The total runtime per execution of the algorithm on the simulated dataset does not exceed 2 minutes, demonstrating its low computational complexity and potential for practical application on large-scale EHR datasets.

4 Comprehensive Analyses of Longitudinal EHR Data in Acute Kidney Injury Patients

Acute Kidney Injury (AKI) is a common clinical condition characterized by an abrupt decline in kidney function, resulting from various causes such as decreased renal perfusion, direct

nephron injury, or urinary tract obstruction [36]. AKI can develop rapidly within hours or days and is associated with significant morbidity and high mortality rates [37]. This syndrome is highly heterogeneous, and the complexity of its pathophysiology poses significant challenges in developing effective patient treatment plans [37].

In this study, we utilize longitudinal EHR data from AKI patients to demonstrate that our proposed method effectively aligns observed EHR records among different subjects who belong to the same cluster. Specifically, we employ unsupervised learning techniques, complemented by clinical evaluations and supervised learning, to validate the effectiveness of our subtype-aware EHR registration method.

4.1 Experimental Setup

Dataset and Cohort Selection We conduct our real data analysis using the Medical Information Mart for Intensive Care (MIMIC)-IV database [38, 39]. The MIMIC-IV dataset contains comprehensive information on over 40,000 patients admitted to intensive care units (ICUs) at the Beth Israel Deaconess Medical Center (BIDMC) between 2008 and 2019. This dataset includes a wide range of clinical data such as demographics, vital signs, laboratory results, procedures, diagnoses, and medications.

To select our cohort of patients with Acute Kidney Injury (AKI), we identified ICU stays where patients had ICD (International Classification of Diseases) codes linked to acute kidney failure, ensuring that the accompanying text explanations contained the keyword “acute kidney injury.” We excluded patients who, during their ICU stay, were labeled with burns, had end-stage renal disease, or renal dialysis. Additionally, patients with an estimated glomerular filtration rate (eGFR) of less than 15 mL/min/1.73 m² were excluded to avoid including those with end-stage renal disease [40].

For data quality assurance, we removed ICU stays with fewer than 15 recorded measurements within the first 21 days after ICU admission. Furthermore, we excluded ICU

stays that had two or fewer recorded measurements in each of the following intervals since ICU admission: 0–7 days, 7–14 days, and 14–21 days. The key feature used in our analysis was serum creatinine levels, a laboratory measurement that is the primary determinant for diagnosing and monitoring AKI [41].

Data Preprocessing and Model Selection We perform unsupervised learning on the data. Specifically, we transform the original longitudinal data as detailed in Section 2, and used the estimated coefficients of the spline basis functions to represent each ICU stay. We applied k -means clustering [42] and k -medoids clustering [43] on these representations. The quality of the resulting clusters was evaluated by computing the average Silhouette coefficient [34].

For clinical evaluation, we labeled each ICU stay based on the AKI severity stages defined below [41, 44]:

1. **Stage 1:** Serum creatinine (SCr) level rises to $1.5\times$ to $1.9\times$ the baseline value within seven days since time 0.
2. **Stage 2:** SCr level rises to $2.0\times$ to $2.9\times$ the baseline value within seven days since time 0.
3. **Stage 3:** SCr level rises to $3\times$ or greater than the baseline value within seven days, or the maximum SCr level over two days is ≥ 4.0 mg/dL. We further divide Stage 3 into two subtypes [44]:
 - (a) **Subtype 1:** SCr level ≥ 4.0 mg/dL within 48 hours since time 0.
 - (b) **Subtype 2:** SCr level rises to $3\times$ or greater than the baseline value within seven days since time 0 and does not meet the criteria for Subtype 1.

The baseline SCr value was computed using the Modification of Diet in Renal Disease (MDRD) equation [45].

We also perform supervised learning on the data. We specifically organize the original longitudinal EHR data into an $N \times T$ array, where N is the number of ICU stays and T represents the number of days since ICU admission. We performed data normalization and missing data imputation following the methods described in [46]. We computed summary statistics (maximum, minimum, mean, standard deviation, and skewness) over 3-day and 4-day windows and performed severe AKI prediction using logistic regression, based on the methods described in [47]. We defined *severe AKI* as observing a $3\times$ increase in creatinine level compared to the baseline value or observing any creatinine level ≥ 4.0 mg/dL during the whole observed time interval of 21 days [41].

4.2 Unsupervised Learning – Phenotyping

We first evaluate the impact of timeline registration on clustering AKI ICU stays using k -medoids and k -means. The average Silhouette coefficients for different number of clusters $K \in [2, 8]$ are presented in Table 2. Notably, when $K = 2$ and $K = 3$, the clustering results yield significantly higher average Silhouette coefficients, indicating more distinct clustering results. Additionally, we observe that both k -medoids and k -means show substantial increases in the average Silhouette coefficients after applying the proposed timeline registration method. Given the heterogeneity of AKI, we expect the ICU stays to cluster according to different subtypes of the condition. The numerical results demonstrate the effectiveness of our timeline registration method in aligning the timelines of patients within the same subtype.

In computational phenotyping research, the number of subtypes K is often unknown and must be determined. Therefore, we consider a scenario in which the number of clusters falls within a pre-specified range, and we apply the proposed timeline registration method to determine this number in a data-driven manner. In Table 3, we present results for two scenarios: one requiring a smaller number of clusters and the other requiring a larger number,

	<i>k</i> -medoids		<i>k</i> -means	
	Observed Data	Registered Data	Registered Data	Registered Data
K=2	0.431	0.483	0.584	0.628
K=3	0.226	0.260	0.523	0.545
K=4	0.249	0.269	0.325	0.332
K=5	0.208	0.280	0.350	0.380
K=6	0.208	0.271	0.352	0.395
K=7	0.111	0.112	0.346	0.402
K=8	0.108	0.159	0.284	0.220

Table 2: Comparison of average Silhouette coefficients for original and adjusted data after applying the proposed timeline registration method, using *k*-medoids and *k*-means clustering.

as potentially suggested by auxiliary information. In both cases, we observe that data after timeline registration show increased average Silhouette coefficients, indicating that the timeline registration method provides consistent improvement in downstream clustering performance.

	<i>k</i> -medoids		<i>k</i> -means	
	Observed Data	Registered Data	Observed Data	Registered Data
$K \in [2, 4]$	0.431	0.483	0.584	0.628
$K \in [5, 8]$	0.208	0.283	0.352	0.431

Table 3: Comparison of average Silhouette coefficients for original and adjusted data after applying the proposed timeline registration method, using *k*-medoids and *k*-means clustering. Number of clusters K is either in the range of $[2, 4]$ or $[5, 8]$.

4.3 Clinical Evaluation

Next, we incorporate clinical information, specifically the AKI severity stages, into the evaluation of timeline registration performance. Recall that the definition of AKI severity stages, as outlined in Section 4.1, relies on the starting time point. This implies that the AKI severity stage of an individual subject may change after applying timeline registration. Therefore, for both the observed data (without timeline registration) and the data after applying the proposed timeline registration procedure, we label each subject as Stage 1 (S1), Stage 2 (S2), Stage 3 Subtype 1 (S3-1), or Stage 3 Subtype 2 (S3-2). We then group both the observed and registered datasets into five different configurations, as described in the first column of Table 4, and evaluate the average Silhouette coefficient for each configuration. The results for these five different AKI sub-category divisions are presented in Table 4. Consistently, the data processed through timeline registration demonstrate an increased average Silhouette coefficient, indicating improved data aggregation within each AKI sub-category.

	Observed Data	Registered Data
4-Groups (S1, S2, S3-1, S3-2)	-0.049	-0.041
3-Groups (S1, S2, (S3-1, S3-2))	-0.057	-0.047
3-Groups ((S1, S2), S3-1, S3-2)	0.286	0.327
2-Groups ((S1, S2), (S3-1, S3-2))	0.321	0.341
2-Groups ((S1, S2, S3-1), S3-2)	0.527	0.627

Table 4: Comparison of observed and recovered data after registration in the clinical setting using new criteria for defining creatinine baseline level.

4.4 Supervised Learning – Severe AKI Prediction

To validate the effectiveness of timeline registration in enhancing downstream clinical analysis, we perform severe AKI¹ prediction and compare the performance using observed data and the recovered data after registration. The experiment was conducted 500 times and we report the mean value with its 95% confidence interval, presented in Table 5 and Table 6.

	Observed Data	Registered Data (k -medoids)	Registered Data (k -means)
AUROC	0.8050 [0.7836, 0.8272]	0.8504 [0.8316, 0.8688]	0.8456 [0.8242, 0.8658]
Accuracy	0.8164 [0.8015, 0.8309]	0.8343 [0.8207, 0.8487]	0.8278 [0.8138, 0.8419]
AUPRC	0.8023 [0.7812, 0.8237]	0.8379 [0.8199, 0.8572]	0.8289 [0.8081, 0.8499]

Table 5: Comparisons of severe AKI prediction using 3-day observed data and recovered data after registration. Metrics are presented using mean values with 95% confidence intervals.

From both tables, we observe that using data after registration results in significant increases in the AUROC (area under the receiver operating characteristic curve) and AUPRC (area under the precision-recall curve) values. Accuracy values also slightly increase. This comparison indicates that timeline registration is influential in enhancing downstream clinical analysis and can be considered an essential preprocessing step.

5 Discussions and Conclusions

In this paper, we demonstrate the necessity of performing timeline registration for longitudinal EHR data, aligning patient records to reflect the intrinsic disease progression trends. To evaluate the feasibility of the proposed registration algorithm for recovering ground truth longitudinal data, we performed simulations with six different scenarios. The results indicate

¹See definition of severe AKI in Data Preprocessing and Model Section in Section 4.1.

	Observed Data	Registered Data (k -medoids)	Registered Data (k -means)
AUROC	0.8276 [0.8062, 0.8489]	0.8787 [0.8621 , 0.8957]	0.8776 [0.8587, 0.8972]
Precision	0.8138 [0.7894, 0.8374]	0.8318 [0.8116 , 0.8548]	0.8251 [0.8035, 0.8449]
Recall	0.7326 [0.7104, 0.7543]	0.7684 [0.7451 , 0.7903]	0.7581 [0.7372, 0.7807]
Accuracy	0.8273 [0.8125, 0.8412]	0.8463 [0.8323 , 0.8604]	0.8403 [0.8261, 0.8546]
AUPRC	0.8256 [0.8046, 0.8460]	0.8680 [0.8509 , 0.8861]	0.8621 [0.8433, 0.8806]

Table 6: Comparisons of severe AKI prediction using 4-day observed data and recovered data after registration. Metrics are presented using mean values with 95% confidence intervals.

that the proposed method can effectively recover observed data to ground truth with low time complexity. To demonstrate the impact of registration on downstream clinical data analysis, we perform clustering with clinical evaluation and severe AKI prediction and compare their results using data with or without timeline registration. The results suggest that registration can effectively improve the performance of downstream clinical data analysis. We also conclude that the registration algorithm is of high stability, reflected by the minimal 95% confidence intervals given 500 times repetition of experiments. Additionally, our proposed registration algorithm has great generalizability in that its clustering step can be substituted by any desired clustering method. Registration on continuous space and evaluation of registration on other critical medical events will be investigated in our future work. EHR timeline registration is an emerging field and our work provides insight for improving clinical analysis using EHR data.

References

- [1] Benjamin Shickel, Patrick James Tighe, Azra Bihorac, and Parisa Rashidi. Deep ehr: A survey of recent advances in deep learning techniques for electronic health record (ehr)

- analysis. IEEE Journal of Biomedical and Health Informatics, 22:1589–1604, 2017.
- [2] Pranjul Yadav, Michael S. Steinbach, Vipin Kumar, and György J. Simon. Mining electronic health records: A survey. ACM Computing Surveys (CSUR), 50(6):85, 2018.
- [3] Duncan Shillan, Jonathan A. C. Sterne, Alan R. Champneys, and Ben Gibbison. Use of machine learning to analyse routinely collected intensive care unit data: a systematic review. Critical Care, 23:284, 2019.
- [4] Antoni Torres, Catia Cillóniz, Michael S. Niederman, Rosario Menéndez, James D. Chalmers, Richard G. Wunderink, and Tom van der Poll. Pneumonia. Nature Reviews Disease Primers, 7:25, 2021.
- [5] Rebecca Irlmeier, Jacob J. Hughey, Lisa Bastarache, Joshua C. Denny, and Qingxia Chen. Cox regression is robust to inaccurate ehr-extracted event time: an application to ehr-based gwas. Bioinformatics, 38:2297–2306, March 2022. doi: 10.1093/bioinformatics/btac086.
- [6] Jane-Ling Wang, Jeng-Min Chiou, and Hans-Georg Müller. Functional data analysis. Annual Review of Statistics and its application, 3:257–295, 2016.
- [7] James Stephen Marron, James O Ramsay, Laura M Sangalli, and Anuj Srivastava. Functional data analysis of amplitude and phase variation. Statistical Science, pages 468–484, 2015.
- [8] J. O. Ramsay and Xiaochun Li. Curve registration. Journal of the Royal Statistical Society Series B: Statistical Methodology, 60(2):351–363, 2002.
- [9] Hiroaki Sakoe and Seibi Chiba. Dynamic programming algorithm optimization for spoken word recognition. IEEE transactions on acoustics, speech, and signal processing, 26(1):43–49, 1978.

- [10] Kongming Wang and Theo Gasser. Synchronizing sample curves nonparametrically. Annals of Statistics, pages 439–460, 1999.
- [11] William H Lawton and Edward A Sylvestre. Self modeling curve resolution. Technometrics, 13(3):617–633, 1971.
- [12] Alois Kneip and Theo Gasser. Convergence and consistency results for self-modeling nonlinear regression. The Annals of Statistics, pages 82–112, 1988.
- [13] Fang Yao, Hans-Georg Müller, and Jane-Ling Wang. Functional data analysis for sparse longitudinal data. Journal of the American statistical association, 100(470):577–590, 2005.
- [14] Alois Kneip and James O. Ramsay. Combining registration and fitting for functional models. Journal of the American Statistical Association, 103:1155–1165, 2008.
- [15] Gareth M James. Curve alignment by moments. The Annals of Applied Statistics, 1(2):480, 2007.
- [16] Laura M Sangalli, Piercesare Secchi, Simone Vantini, and Alessandro Veneziani. A case study in exploratory functional data analysis: geometrical features of the internal carotid artery. Journal of the American Statistical Association, 104(485):37–48, 2009.
- [17] Anuj Srivastava, Wei Wu, Sebastian Kurtek, Eric Klassen, and J. S. Marron. Registration of functional data using fisher-rao metric. arXiv, 1103.3817, 2011.
- [18] J Derek Tucker, Wei Wu, and Anuj Srivastava. Generative models for functional data using phase and amplitude separation. Computational Statistics & Data Analysis, 61: 50–66, 2013.
- [19] Wei Wu and Anuj Srivastava. Analysis of spike train data: Alignment and comparisons using the extended fisher-rao metric. Electronic Journal of Statistics, 8:1776–1785, 2014.

- [20] Julia Wrobel, Vadim Zipunnikov, Jennifer Schrack, and Jeff Goldsmith. Registration for exponential family functional data. Biometrics, 75(1):48–57, 2019.
- [21] Julia Wrobel. Register: Registration for exponential family functional data. Journal of Open Source Software, 3(22):557, 2018.
- [22] Julia Wrobel and Alexander Bauer. registr 2.0: Incomplete curve registration for exponential family functional data. Journal of Open Source Software, 6(61):2964, 2021.
- [23] Rong Tang and Hans-Georg Müller. Pairwise curve synchronization for functional data. Biometrika, 95(4):875–889, 2008.
- [24] Jie Peng, Debashis Paul, and Hans-Georg Müller. Time-warped growth processes, with applications to the modeling of boom–bust cycles in house prices. The Annals of Applied Statistics, 8:1561–1582, 2014.
- [25] Erin I McDonnell, Vadim Zipunnikov, Jennifer A Schrack, Jeff Goldsmith, and Julia Wrobel. Registration of 24-hour accelerometric rest-activity profiles and its application to human chronotypes. Biological rhythm research, 53(8):1299–1319, 2022.
- [26] Pantelis Z Hadjipantelis, John AD Aston, Hans-Georg Müller, and Jonathan P Evans. Unifying amplitude and phase analysis: A compositional data approach to functional multivariate mixed-effects modeling of mandarin chinese. Journal of the American Statistical Association, 110(510):545–559, 2015.
- [27] Xueli Liu and Mei-Cheng K. Yang. Simultaneous curve registration and clustering for functional data. Computational Statistics & Data Analysis, 53(4):1361–1376, 2009.
- [28] Zizhen Wu and David B. Hitchcock. A bayesian method for simultaneous registration and clustering of functional observations. Computational Statistics & Data Analysis, 101:121–136, 2016.

- [29] Shiyi Jiang, Rungang Han, Krishnendu Chakrabarty, David Page, William W Stead, and Anru R Zhang. Timeline registration for electronic health records. AMIA Jt Summits Transl Sci Proc, 2023:291–299, 2023. PMID: 37350882; PMCID: PMC10283114.
- [30] Milos Hauskrecht, Iyad Batal, Michal Valko, Shyam Visweswaran, Gregory F Cooper, and Gilles Clermont. Outlier detection for patient monitoring and alerting. Journal of biomedical informatics, 46(1):47–55, 2013.
- [31] Grace Wahba. Spline Models for Observational Data. CBMS-NSF Regional Conference Series in Applied Mathematics. Society for Industrial and Applied Mathematics, Philadelphia, PA, 1990.
- [32] Trevor Hastie, Robert Tibshirani, Jerome H Friedman, and Jerome H Friedman. The elements of statistical learning: data mining, inference, and prediction, volume 2. Springer, 2009.
- [33] Grace Wahba and Yuedong Wang. Spline functions: Overview. Wiley StatsRef: Statistics Reference Online, pages 1–19, 2014.
- [34] Peter J Rousseeuw. Silhouettes: a graphical aid to the interpretation and validation of cluster analysis. Journal of computational and applied mathematics, 20:53–65, 1987.
- [35] Xin Jin and Jiawei Han. K-Medoids Clustering, pages 564–565. Springer US, Boston, MA, 2010. ISBN 978-0-387-30164-8. doi: 10.1007/978-0-387-30164-8_426. URL https://doi.org/10.1007/978-0-387-30164-8_426.
- [36] Konstantinos Makris and Loukia Spanou. Acute kidney injury: Definition, pathophysiology and clinical phenotypes. The Clinical biochemist. Reviews, 37(2):85–98, 2016.
- [37] Oleksa G. Rewa and Sean M. Bagshaw. Acute kidney injury—epidemiology, outcomes and economics. Nature Reviews Nephrology, 10:193–207, 2014.

- [38] Ary L. Goldberger, Luis A. Nunes Amaral, L Glass, Jeffrey M. Hausdorff, Plamen Ch. Ivanov, Roger G. Mark, Joseph E. Mietus, George B. Moody, Chung-Kang Peng, and Harry Eugene Stanley. Physiobank, physiokit, and physionet: components of a new research resource for complex physiologic signals. Circulation, 101(23):E215–20, 2000.
- [39] Alistair E. W. Johnson, Lucas Bulgarelli, Lu Shen, Alvin Gayles, Ayad Shammout, Steven Horng, Tom J. Pollard, Benjamin Moody, Brian Gow, Li wei H. Lehman, Leo Anthony Celi, and Roger G. Mark. MIMIC-IV, a freely accessible electronic health record dataset. Scientific Data, 10:1, 2023.
- [40] Xing Song, Alan SL Yu, John A Kellum, Lemuel R Waitman, Michael E Matheny, Steven Q Simpson, Yong Hu, and Mei Liu. Cross-site transportability of an explainable artificial intelligence model for acute kidney injury prediction. Nature Communications, 11:5668, 2020. doi: 10.1038/s41467-020-19551-w.
- [41] Arif Khwaja. Kdigo clinical practice guidelines for acute kidney injury. Nephron Clinical Practice, 120:c179–c184, 2012.
- [42] James MacQueen. Some methods for classification and analysis of multivariate observations. In Proceedings of the Fifth Berkeley Symposium on Mathematical Statistics and Probability, volume 1, pages 281–297. Oakland, CA, USA, 1967.
- [43] LKPJ Rduseeun and P Kaufman. Clustering by means of medoids. In Proceedings of the statistical data analysis based on the L1 norm conference, neuchatel, switzerland, volume 31, 1987.
- [44] Zihan Zhu, Xin Gai, and Anru R. Zhang. Functional post-clustering selective inference with applications to ehr data analysis. arXiv, 2405.03042, 2024.
- [45] Andrew S. Levey, Juan Ponsa Bosch, Julia Breyer Lewis, Tom Greene, Nancy L. Rogers, and David Roth. A more accurate method to estimate glomerular filtration rate from

serum creatinine: A new prediction equation. Annals of Internal Medicine, 130:461–470, 1999.

[46] Shiyi Jiang, Xin Gai, Miriam M. Treggiari, William W. Stead, Yuankang Zhao, David Page, and Anru R. Zhang. Soft phenotyping for sepsis via ehr time-aware soft clustering. Journal of Biomedical Informatics, 152:104615, 2023.

[47] Zachary Chase Lipton, David C. Kale, Charles Peter Elkan, and Randall C. Wetzel. Learning to diagnose with lstm recurrent neural networks. In ICLR, 2016.

6 Appendix

Simulation Results Figures



Figure 3: Simulation 2 trajectories



Figure 4: Simulation 3 trajectories

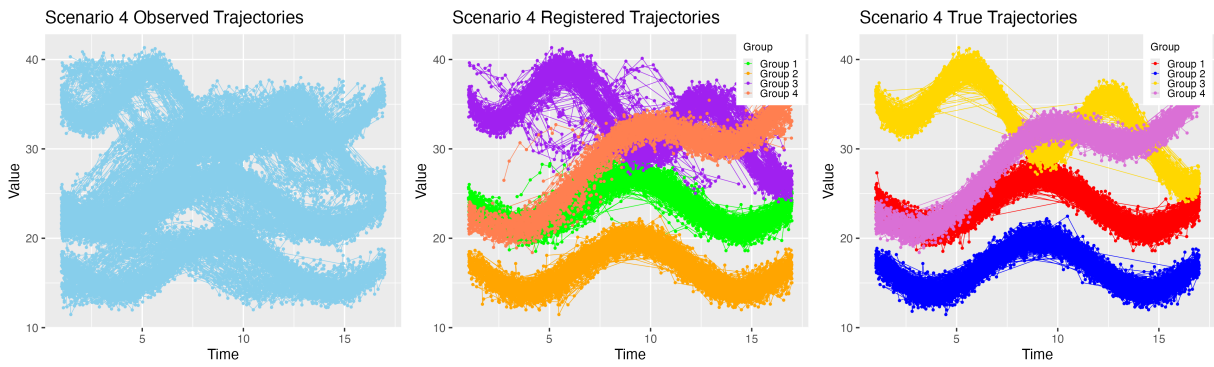


Figure 5: Simulation 4 trajectories

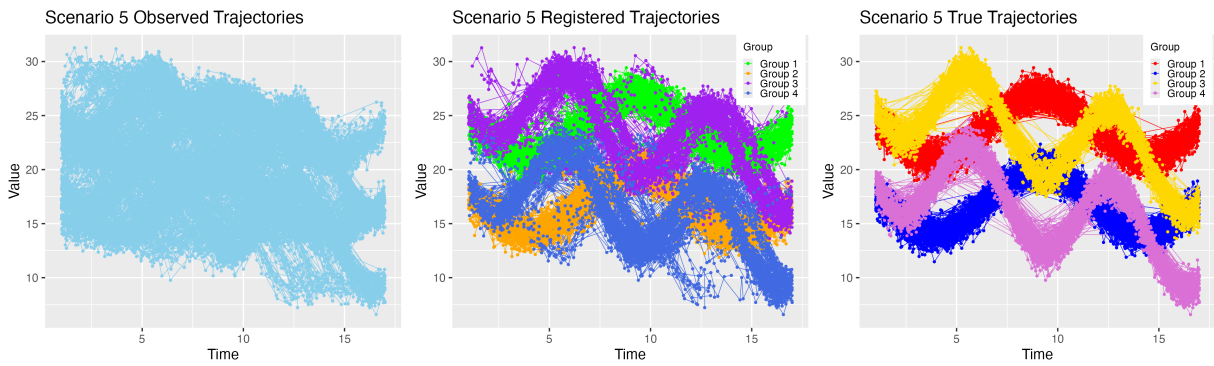


Figure 6: Simulation 5 trajectories

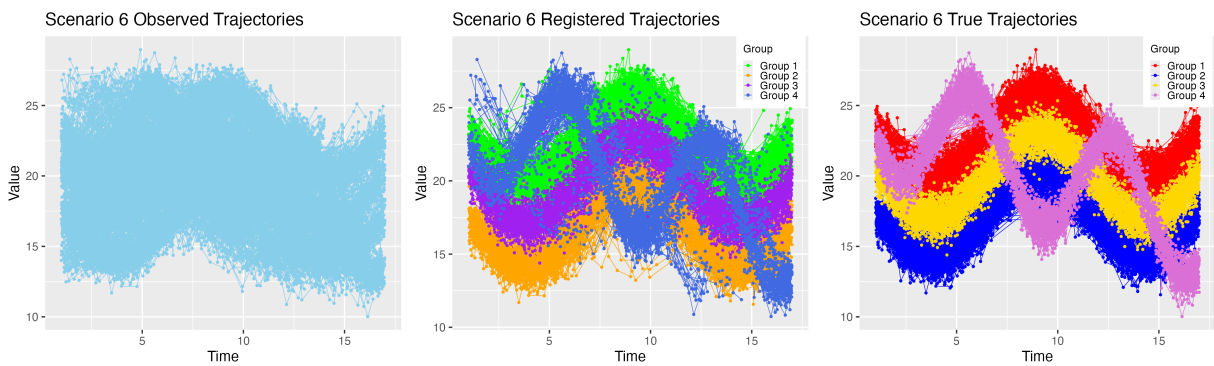


Figure 7: Simulation 6 trajectories